

Determination of the Surfactant Density on SWCNTs by Analytical Ultracentrifugation

Claudia Backes,^[a, b] Engin Karabudak,^[c, d] Cordula D. Schmidt,^[b] Frank Hauke,^[a, b]
Andreas Hirsch,^[a, b] and Wendel Wohlleben*^[d]

Abstract: We report on the extensive characterization of single-walled carbon nanotubes (SWCNTs) dispersed in a variety of surfactants, such as sodium dodecyl benzene sulfonate (SDBS), sodium cholate (SC), and three synthesized perylene-based surfactants, by using differential sedimentation in H₂O and D₂O. Multidimensional evaluation of the absorption profiles over radius, wavelength, and time allows the determination of the anhydrous specific volumes of the SWCNT–surfactant complexes as well as the concentration of the surfactant reser-

voir in free micelles with very slow sedimentation coefficients (<1 Svedberg). Among the perylene bisimide surfactants, the smallest derivative is densely adsorbed on the nanotube backbone with an anhydrous specific volume significantly above that of SC or SDBS. Bulky Newkome dendritic groups on one or both ends of the perylene

moiety gradually reduce the adsorption density, in accord with the absolute adsorption between 0.66 and 1.7 mmol surfactant per gram SWCNTs. Furthermore, hydrodynamic analysis reveals that SDBS favors the “tails-on” configuration. The distribution of sedimentation coefficients of SWCNTs prepared by high-pressure carbon monoxide decomposition (HiPco) is broader and shifted to faster sedimentation than those prepared by using cobalt–molybdenum catalysis (CoMoCAT), which reflects the polydispersity in diameter and length.

Keywords: analytical ultracentrifugation • nanotubes • perylenes • supramolecular chemistry • surfactants

Introduction

The characterization of single-walled carbon nanotubes (SWCNTs) has long been a major challenge in carbon nanotube research due to the polydispersity of the raw material.

In this respect, fractionation by centrifugation has proven to be extremely valuable. The first report on centrifugation of SWCNTs by O’Connell et al. is a significant step forward in nanotube characterization, because the separation of aggregated and isolated nanotubes by removal of SWCNT bundles with centrifugation led to the observation of nanotube near-IR photoluminescence.^[1]


In 2005, another landmark in nanotube centrifugation was reached with the demonstration of the feasibility of nanotube separation according to diameter by using a density gradient.^[2] In density gradient ultracentrifugation (DGU), a sample of surfactant-encapsulated nanotubes is loaded into an aqueous solution with a known density gradient established by a gradient medium, such as iodixanol, nycodenz, or sucrose. Upon applying a centrifugal force, the species travels towards its isopycnic point (the position at which its density is equal to that of the gradient). The spatially separated bands can then be fractionated. DGU is now a well-established method for nanotube separation,^[2–20] especially according to diameter and/or electronic type. Preparative ultracentrifugation is a highly versatile tool that has led to numerous advances in the characterization and application of carbon nanotubes.

[a] C. Backes, Dr. F. Hauke, Prof. Dr. A. Hirsch
Institute of Advanced Materials and Processes (ZMP)
University of Erlangen–Nuremberg, Dr. Mack Strasse 81
90762 Fuerth (Germany)

[b] C. Backes, C. D. Schmidt, Dr. F. Hauke, Prof. Dr. A. Hirsch
Department of Chemistry and Pharmacy
Institute of Organic Chemistry II
University of Erlangen–Nuremberg
Henkestrasse 42, 91054 Erlangen (Germany)

[c] Dr. E. Karabudak
Present address:
MESA+ Research Institute, University of Twente
Meander ME147, 7500AE Enschede (The Netherlands)

[d] Dr. E. Karabudak, Dr. W. Wohlleben
BASF SE, Polymer Physics Research
67056 Ludwigshafen (Germany)
Fax: (+49) 621-60-92281
E-mail: wendel.wohlleben@basf.com

 Supporting information for this article is available on the WWW under <http://dx.doi.org/10.1002/chem.200903461>.

However, quantitative studies on the hydrodynamic properties of surfactant-encapsulated SWCNTs during centrifugation are scarce. Nair et al. used a hydrodynamic model to describe the motion of SWCNTs in a centrifugal field;^[15] however, their study was based on buoyant densities, and the spreading of the nanotubes close to their isopycnic points. Since the buoyant density also includes a large hydration shell, it is not possible to draw conclusions on the mass and volume of the surfactant layer alone.

In an alternative approach, Hersam and co-workers^[21] have characterized the hydrodynamic properties of sodium cholate encapsulated CoMoCAT SWCNTs by using analytical ultracentrifugation (AUC). This allowed a more direct investigation, as the hydration layer that convoluted the results of Nair et al. does not need to be considered in this case, because its density is approximately equal to the density of water. Thus, the sedimentation velocity of a SWCNT–surfactant complex depends on its so-called anhydrous partial specific volume.

The sedimentation velocity of particles in a centrifugal field is determined by the sedimentation and diffusion coefficients, as well as the hydrodynamic frictional coefficients. It can be measured by analytical ultracentrifugation, in which the temporal and spatial distribution of the sedimenting species can be directly detected in situ; for example, by absorption spectroscopy (Figure 1). Other optics such as interference, turbidity, Schlieren, and X-ray are available for in situ detection,^[22,23] but absorption is the most suitable technique for nanotube characterization.

As described by Hersam et al.,^[21] the classical technique of differential sedimentation in H₂O and D₂O^[24,25] can also be applied to nanotubes. The determination of the sedimentation, diffusion, and hydrodynamic frictional coefficients^[26] in H₂O and D₂O enables the calculation of the anhydrous molar volume of the surfactant-encapsulated SWCNTs,

which then allows the linear packing density of the surfactant on the nanotube surface to be determined. Based on these previous observations, the hydrodynamic properties of various SWCNT–surfactant systems have been compared in this study to aid the understanding of the interaction of SWCNTs and surfactant molecules in solution, which is of utmost importance for the design of novel, potent SWCNT dispersants. Using sedimentation rates in water and deuterated water, we have determined the anhydrous specific volume of SWCNTs dispersed in aqueous solutions of the commercially available surfactants sodium cholate (SC) and sodium dodecyl benzene sulfonate (SDBS), as well as three different synthesized perylene-based surfactants.^[27–29] The results of the hydrodynamic characterization of the SWCNT–surfactant complexes agree well with the previously reported adsorption models for SDBS and SC, which demonstrates the versatility of the methodology. Within the series of perylene surfactants, we have now established that molecules of lower molecular weight and lower charge density can be more densely organized onto the nanotube scaffold, which has previously been indicated by zeta potential measurements.^[28]

Results and Discussion

The study described herein is based on the sedimentation rates of SWCNTs prepared by high-pressure carbon monoxide decomposition (HiPco) and SWCNTs prepared by using cobalt–molybdenum catalysis (CoMoCAT) dispersed with the aid of five different surfactants in water and deuterated water. As surfactants we have chosen SC as representative of a bile salt dispersant, SDBS as a traditional micelle-forming surfactant, and three synthesized π -surfactants (**1–3**) with perylene bisimides (Per) as the aromatic anchoring

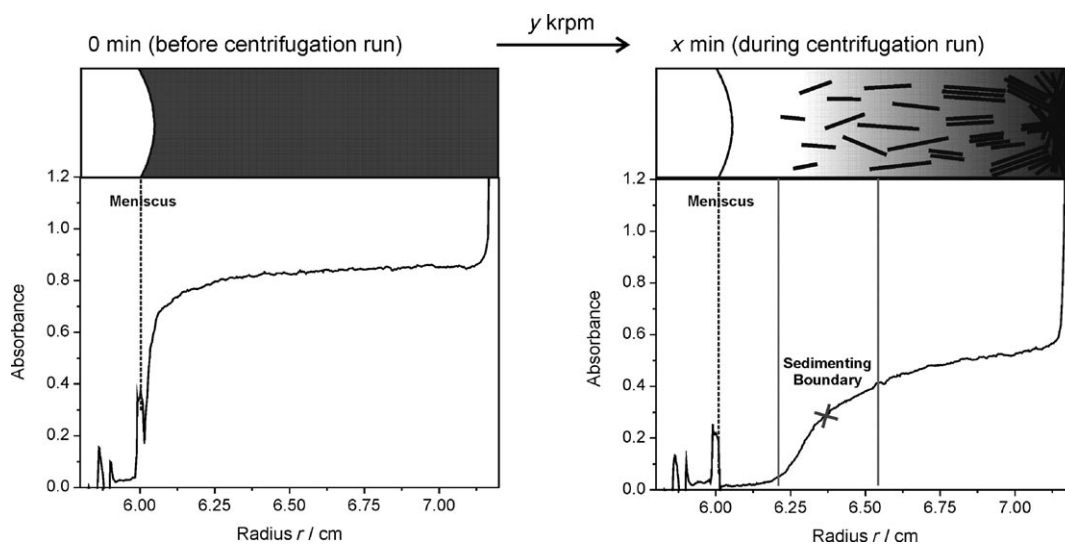
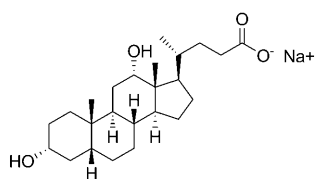
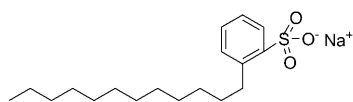


Figure 1. Schematic representation of SWCNTs in an analytical ultracentrifuge cell (top panels) before and at a certain time during the centrifugation. The corresponding plots of optical density versus cell radius are displayed in the bottom graphs. The meniscus of the solution is identified by an artificial peak in the optical density (dashed line) and the sedimenting boundary is found between the vertical solid lines, marked by the symbol \times .^[21]

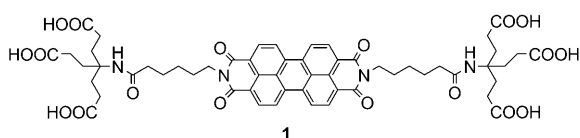
groups, which have been shown to yield highly stable SWCNT dispersions with high degrees of individualization.^[27,28]



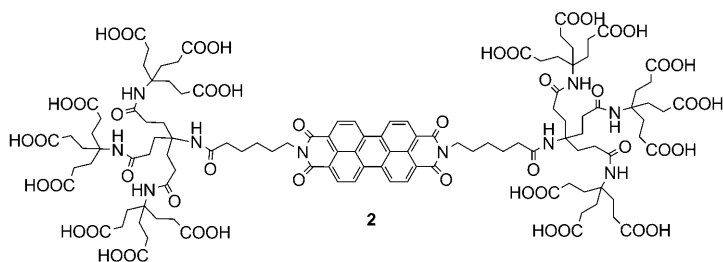
SDC



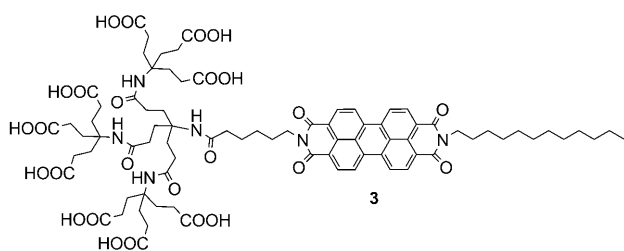
SDBS



1



2



3

The dispersions were prepared by immersing SWCNTs in aqueous solutions of SC and SDBS (10 g L^{-1}) or buffered aqueous solutions (phosphate buffer, pH 7) of the perylene bisimide derivatives ($[\text{Per}]/[\text{SWCNT}]=1:1$). We have focused on SWCNTs produced by HiPco and by CoMoCAT. The dispersions were mildly precentrifuged (30 min, 15000 rpm) to remove coarse aggregates and large SWCNT bundles. The top 70% of the supernatant was collected and, if necessary, diluted with the relevant surfactant solution to give an optical density of approximately 1 cm^{-1} at 740 nm. In contrast to the study of Hersam et al.^[21] the pristine SWCNT material was not sorted by diameter with DGU.

Hydrodynamic fractionation and multidimensional evaluation: The aqueous dispersions were loaded into two-hole Epon cells and subjected to ultracentrifugation at 40 krpm (25°C). The spatial and temporal distribution of the SWCNT–surfactant complex was followed by in situ measurements of the absorbance. The so-determined concentration profiles $c(r, t, \lambda)$ are three dimensional,^[30] and show the expected redistribution during the sedimentation of the nanotubes, as depicted for HiPco–Per3 (H_2O), for example, in Figure 2. Initially, at $t=0$, the concentration of SWCNTs

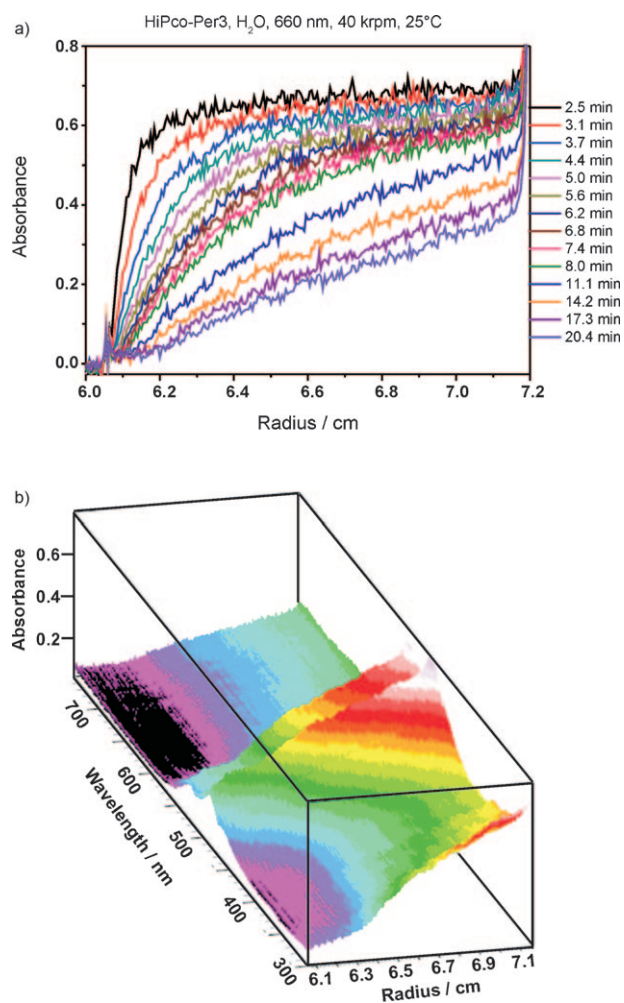


Figure 2. Experimental raw data of HiPco–3 sedimentation at 40 krpm in H_2O . a) Concentration $c(r, t)$ profiles at 660 nm detection. The steep rises at 6.0 and 7.17 cm mark the meniscus and the bottom of the cell, respectively. b) Snapshot of $c(r, \lambda)$ after 32 min. See the Movie S1 in the Supporting Information for the entire temporal evolution of $c(r, t, \lambda)$.

is uniform along the centrifuge cell. During centrifugation, a net sedimentation of the nanotubes occurs from smaller to larger radii so that the top of the cell becomes depleted of nanotubes; that is, the optical density is reduced, which results in the development of a boundary (see the blue trace in Figure 2a). With time, the boundary broadens and moves towards the bottom of the cell (see the black trace). The

temporal snapshot in Figure 2b shows Per-encapsulated nanotubes of around 6.5 cm and Per micelles close to the meniscus at 6 cm. Movie S1 in the Supporting Information allows the successive sedimentation of bundles, individualized nanotubes, and micelles to be visualized. It is in fact the main advantage of the analytical ultracentrifuge that, due to the fractionating measurement principle, small colloids (individualized nanotubes) are characterized without any perturbation from the larger colloids (bundles). Bundles sediment faster than individual nanotubes, so they are removed before sedimentation of the nanotubes can even be detected.

The sedimentation coefficient, s , diffusion, D , and the hydrodynamic frictional coefficient, f (specifically the frictional ratio ff_0) are obtained by fitting the experimental $c(r, t)$ profiles to the multicomponent Lamm equation by using appropriate programs such as SEDFIT^[26,31,32] or Ultrascan.^[33–35] The sedimentation coefficient, s , is an instrument independent measure of the sedimentation speed, u , reduced by the centrifugal acceleration, $s = u/\omega^2 r$, in which ω is the rotational frequency and r the average radius of the measurement cell from the center of rotation ($r = 6.5$ cm in Beckman model XLI machines).^[22,23] The frictional ratio ff_0 compares the frictional force acting on a solute with the frictional force acting on a sphere of equal volume. Any deviation from $ff_0 = 1$ indicates a noncompact, nonspherical morphology.^[22,23] To understand the uncertainties in the evaluation procedure, we discuss their mathematical basis beyond the slightly naïve use of SEDFIT in the nonetheless groundbreaking study by Hersam et al.^[21]

The evaluation first optimizes a volume-weighted distribution of sedimentation coefficients for best fit to the experimental movie of fractionation. In this step, SEDFIT makes use of the temporal evolution of a broadening sedimentation boundary; polydispersity broadens linearly with time, but diffusion broadening varies with the square root of time. Subsequently, a regularization procedure assesses automatically whether small changes of the obtained best fit are statistically relevant on the 0.98 confidence level. The procedure reports, as a final result, the average distribution of all statistically indiscernible distributions.^[26,31] The distribution of sedimentation coefficients $c(s)$ is a robust result, which is over-determined because the apparent coefficient s^* can be obtained from a single snapshot, in which diffusion is neglected. Details of the shape of the $c(s)$ distribution can be deconvoluted from diffusion; that is, they are correlated with the frictional ratios. The frictional ratio is only obtained from global evaluation of the shape evolution of the sedimenting boundary among all snapshots.

A 2D fit of both s and ff_0 multiplies the degrees of freedom and inherently optimizes the quality of the fit. A 2D grid of 10 values for ff_0 and 120 values for s is computationally affordable with less than an hour of fitting time on a standard personal computer. The grid spacing in s is chosen to be logarithmic to enhance the resolution and the fitting penalty by quadratic deviation in the region of the individualized nanotubes. Results for ff_0 depend on the rotational frequency chosen for the experiment, because the relative influence of polydispersity and diffusion on the boundary broadening changes with the effective duration of the experiment. The anhydrous specific volume \bar{v} is another caveat. It is experimentally derived from comparison of the sedimentation coefficient s in H₂O and D₂O, but before that, \bar{v} must be specified in the fit to obtain the sedimentation coefficients. We set \bar{v} to 0.5 cm³g⁻¹ in the fits, but we also confirmed that identical results are obtained for \bar{v} of 0.3 and 0.8 cm³g⁻¹.

A typical result is shown in Figure 3. We consistently obtain larger values of ff_0 for the first peak of slowly sedimenting signals, which can be identified with individualized

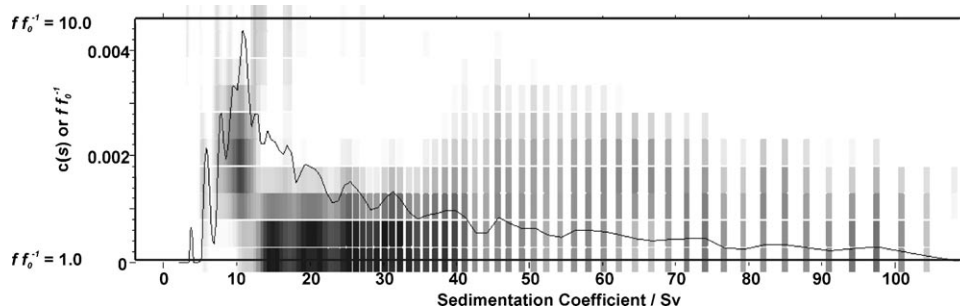


Figure 3. 2D results of frictional ratio (shaded areas) and sedimentation coefficient (black trace) for HiPco-SC in D₂O. The individualized CNTs have a clearly extended configuration with ff_0 around 5, whereas the entangled CNTs have a more compact morphology with lower ff_0 . The fitting range for s was 2–120 Sv (log spacing) with ff_0 from 1–10.

nanotubes. We integrate over this peak only, for all subsequent evaluations, thus removing any contribution by bundles. Note that this option is not available in ensemble methods such as fluorescence spectroscopy, dynamic light scattering, zeta-potential, small-angle X-ray scattering, and small-angle neutron scattering. For all our experiments, we find an average $ff_0 = 4.8 \pm 1.8$ (H₂O) and 3.8 ± 1.6 (D₂O) for the individualized nanotubes, which are significantly different from each other. The average of the differences is even larger, with 40% deviation between the frictional ratios fitted from H₂O and D₂O experiments of the same nanotube-surfactant system. This indicates weak reliability of the shape analysis. Unfortunately, the combined uncertainty from the sedimentation coefficient and the frictional ratio leads to an even larger average deviation (55%) in the molar masses from H₂O and D₂O experiments. The reason for the discrepancies is the stronger influence of diffusion in the D₂O experiment (all at the same rotational speed),

giving SEDFIT the mathematical freedom to model diffusion by low masses alone. Hersam et al. indicate that their experiments were performed at only 27 krpm, which we believe to be a typographical error, because we tested that individualized nanotubes with sedimentation coefficients of around 10 Svedberg do not even form a boundary at such a low speed. In principle, experiments in both solvents should be conducted at several rotational speeds (e.g., 35, 45, and 55 krpm), and evaluated globally to decrease the uncertainty in the shape analysis. SEDFIT does not offer $c(s, f/f_0)$ shape analysis for multiple datasets, but the (only) alternative evaluation platform Ultrascan does.^[34,35] However, Ultrascan shape analysis requires supercomputer facilities for the 2D Genetic Algorithm fit, and was hence not used for the present large series of experiments.

As a cross-check for the SEDFIT results, a single dataset of the present study (HiPco-SC-D₂O) was evaluated in Ultrascan with the van Holde–Weischet and 2D Genetic Algorithm on the UTHSCSA Texas Supercomputer Facility. This gave exact confirmation of the sedimentation coefficients $c(s)$, but considerably lower values for the frictional coefficient of the individualized nanotubes. This further strengthens our reservations against hydrodynamic modeling based on $c(s, s, f/f_0)$ shape results.

In the majority of our experiments, we used the commercial XLA machine, with which only single wavelengths can be recorded. In this case, we chose to follow the spatial and temporal distribution of the sedimenting species at a wavelength of 550 nm. At this wavelength, we captured both the nanotubes and the perylene surfactants in a single measurement (see absorption spectra in Figures S2 and S3 in the Supporting Information), but not the SC or SDBS surfactant micelles. Figure S4 in the Supporting Information depicts the $c(s)$ distributions of HiPco–Per2 at three different wavelengths (550, 650, and 750 nm). Very little difference in the regime of the sedimentation coefficients attributed to the nanotube species (>10 Sv) is discernable. This is to be expected for the broad absorption spectrum of nanotubes. However, at 550 nm and 650 nm, very slowly sedimenting species (presumed to be free perylene micelles) are present. Thus, at a suitable wavelength, such as 550 nm, the hydrodynamic characterization of the free surfactant and the nanotube surfactant complexes can be carried out in a single experiment.

Comparison of HiPco and CoMoCAT in surfactant complexes: Table 1 gives an overview of the sedimentation coefficients s , the anhydrous molar masses M , the frictional ratios f/f_0 and the anhydrous specific volumes \bar{v} of the SWCNT–surfactant complexes investigated.

From the sedimentation coefficients in water and deuterated water, the anhydrous specific volumes of the SWCNT–surfactant complexes can be calculated. These results are also summarized in Table 1. Based on the assumption of equivalent surfactant adsorption in water and deuterated water (which is quite reasonable, because surfactant adsorption on the nanotube scaffold is mainly driven by the hydro-

Table 1. Tabulated data of the sedimentation coefficients s , frictional ratios f/f_0 , anhydrous molar mass M , and anhydrous specific volume \bar{v} of the systems investigated.

		s [Sv]	$M^{[a]}$ [kDa]	f/f_0	\bar{v} [cm ³ g ⁻¹]
CoMoCAT–SC	H ₂ O	13.0	750	5.4	0.56
	D ₂ O	9.2	440	3.8	
HiPco–SC	H ₂ O	16.6	500	2.9	0.65
	D ₂ O	10.9	860	5.1	
HiPco–SDBS	H ₂ O	15.4	1500	6.4	0.83
	D ₂ O	6.1	210	3.6	
HiPco–Per1	H ₂ O	26.6	770	2.7	0.81
	D ₂ O	11.8	440	3.0	
HiPco–Per2	H ₂ O	18.7	2700	4.2	0.69
	D ₂ O	11.7	510	1.3	
HiPco–Per3	H ₂ O	25.8	1600	7.0	0.75
	D ₂ O	14.8	1100	5.7	

[a] Anhydrous molar mass.

phobic effect), the anhydrous specific volume \bar{v} can be expressed as shown in Equation (1) in which η is the viscosity of the solvent, ρ is its density, and the subscripts H and D denote water and deuterated water, respectively:

$$\bar{v} = \frac{\eta_{\text{H}}S_{\text{H}} - \eta_{\text{D}}S_{\text{D}}}{\eta_{\text{H}}S_{\text{H}}\rho_{\text{D}} - \eta_{\text{D}}S_{\text{D}}\rho_{\text{H}}} \quad (1)$$

Before discussing subtle differences in the sedimentation coefficients with various nanotube surfactants, the sedimentation velocities in water and deuterated water deserve some attention. In all cases, the sedimentation velocity in D₂O is much slower than in H₂O (Figure 4). This can be attributed to the fact that the density of dispersed individualized SWCNTs is greater than one, so that it matches the density of D₂O (1.104 g cm⁻³ at 25 °C) more closely than the density of water (0.998 g cm⁻³). The anhydrous densities of the individualized component of the SWCNT–surfactant dispersions are measured to be between 1.1–1.8 g cm⁻³ (the density is inversely proportional to the anhydrous specific volume summarized in Table 1).

Interestingly, the amount of bundled SWCNT species appears to be reduced for the samples dispersed in deuterated water, as the peaks with higher sedimentation coefficients are smaller than the main peak of the individualized nanotubes. This is especially striking in the $c(s)$ distribution of CoMoCAT–SC (Figure 4a). This impression is further supported by the observation that all samples in D₂O have intrinsically been of higher optical density; for example, higher nanotube concentration after the first centrifugation step than the samples prepared in water, although the initial nanotube concentration was constant. Further investigations concerning this phenomenon are currently underway in our laboratory.

Upon comparing the HiPco to the CoMoCAT pristine material, striking differences appear in the $c(s)$ distributions, as shown for SWCNT–SC in (Figure 5). First of all, the s -value distribution attributed to the individualized nanotubes is much broader for the HiPco material than for the CoMoCAT SWCNTs. This is not surprising, because the diameter

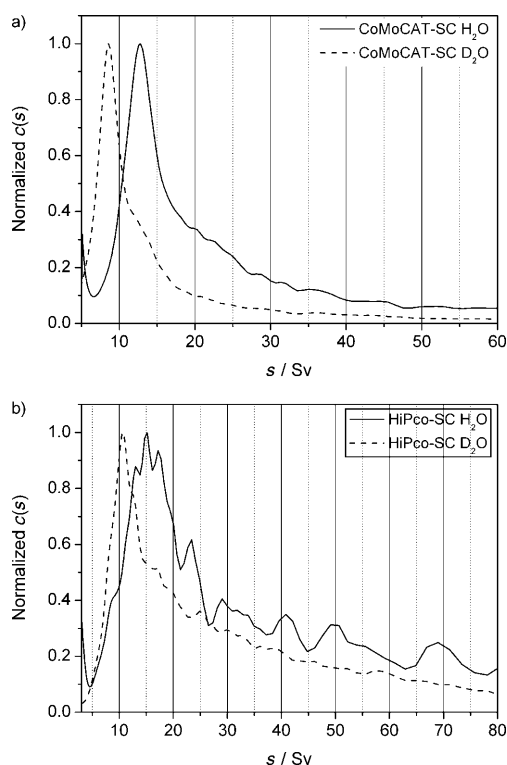


Figure 4. $c(s)$ distribution for a) CoMoCAT-SC in H_2O and D_2O and b) HiPco-SC in H_2O and D_2O derived from fitting the experimental data from the XLA with the model of continuous $c(s)$ distribution with logarithmic steps from 5 to 130 Sv and \bar{v} set to 0.6 and f/f_0 to 5.

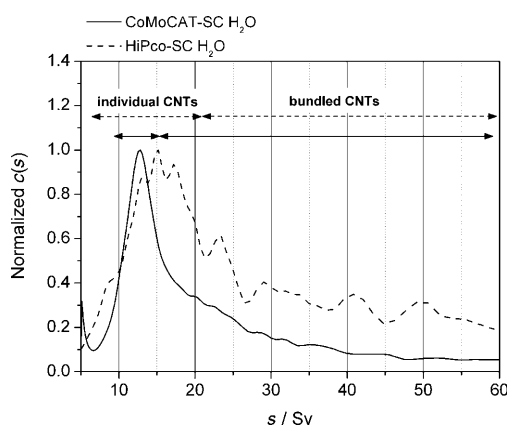


Figure 5. $c(s)$ distribution for CoMoCAT-SC and HiPco-SC in H_2O derived from fitting the experimental data from the XLA with the model of continuous $c(s)$ distribution.

(and length) distribution of the HiPco sample ranges from 0.8–1.4 nm, whereas it is much narrower for the CoMoCAT nanotubes (0.7–0.9 nm). Thus, HiPco SWCNTs are characterized on average by a broader s -value distribution and higher sedimentation coefficients.

The application of hydrodynamic models such as the “smooth surfactant cylinder” of Hersam et al. is questionable in light of the given uncertainties in the experimental values for f/f_0 and M . Furthermore, those surfactants that do

not collapse flat onto the nanotube surface do not match the flat-cylinder model, and negative values (which have no physical meaning) for the ligand packing density appear. In contrast, the anhydrous specific volume \bar{v} is a reliable result that involves little modeling, and results directly from the overdetermined sedimentation coefficients.

To determine \bar{v} , we used the model of Hersam et al.,^[21] but corrected Formulae 8, 9c, and 10c to match molecular and molar units on both sides of the equation.

Geometry of SWCNT-complexes with various surfactants:

In the following, comparisons of the anhydrous specific volumes of the SWCNT-surfactant complexes are drawn as a foundation for understanding the underlying noncovalent interactions. Regarding the classical surfactants SC and SDBS, significant differences in the anhydrous molar volumes \bar{v} of the HiPco-surfactant complexes have been determined. For example, \bar{v} of the HiPco-SDBS complex is much greater than for the HiPco-SC complex.

The adsorption of SC has already extensively been studied in the AUC investigation of Hersam and co-workers.^[21] It was shown that SC is densely packed on the nanotube surface with a linear surfactant density of 3.6 molecules per nm of SWCNT surface. The six-membered carbon rings are believed to stack at the nanotube sidewall with the nonpolar side (without hydroxyl functionalities) facing the SWCNT surface (Figure 6).

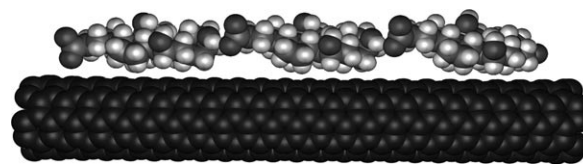


Figure 6. Schematic representation of the adsorption of sodium cholate molecules on the surface of a (6,5) nanotube.

From the anhydrous diameter of the (6,5)-SWCNT-SC complex (1.8 nm) and the diameter of the (6,5)-nanotube (0.75 nm), the diameter contribution of one adsorbed surfactant molecule is deduced to be 0.53 nm.

In contrast to SC, the adsorption of SDBS is strongly dependent on the concentration of the surfactant. Even though it has been demonstrated that SDBS is capable of dispersing SWCNTs even at 0.1 cmc (cmc = 1.2 mM = 0.4 g L⁻¹),^[36] the concentration of SDBS is most commonly kept higher (10–20 g L⁻¹) as the debundling is more efficient at concentrations of around 14 g L⁻¹ (33 × cmc).^[37] This observation can be attributed to the fact that the orientation of the SDBS molecules on the nanotube surface can either be in the so-called “tails-on” conformation (see Figure 7a) or “head-to-tail”, with the SDBS molecules arranged parallel to the nanotube surface (see Figure 7b). At low SDBS concentrations the head-to-tail configuration is favored, whereas the SDBS molecules tend to “stand upright” at higher concentrations.

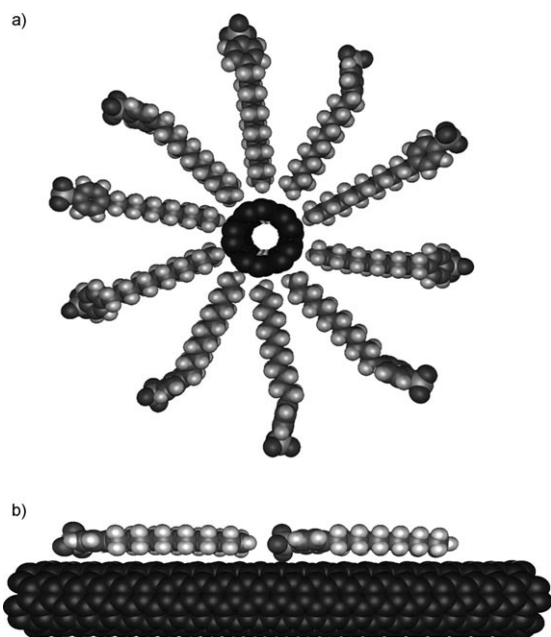


Figure 7. Schematic illustration of the possible adsorption mechanisms of SDBS on a graphitic surface; a) “tails-on” configuration, b) “head-to-tail” conformation.

In our case, an SDBS concentration of 10 g L^{-1} was chosen so that, theoretically, the tails-on configuration would be favored. In this case the diameter of SWCNT-SDBS is expected to be approximately $d(\text{SWCNT}) + 2 \cdot (2.4 \text{ nm}) + \text{van der Waals distance}$, whereas for SWCNT-SC it is $d(\text{SWCNT}) + 2(0.53 \text{ nm})$.^[36,37] This agrees well with the calculated anhydrous specific molar volume derived from the sedimentation coefficients in water and deuterated water, as \bar{v} (HiPco-SC) was found to be $0.63 \text{ cm}^3 \text{ g}^{-1}$, in comparison with $0.83 \text{ cm}^3 \text{ g}^{-1}$ for HiPco-SDBS (Table 1). However, in addition to the nanotube and SDBS concentrations, the nanotube diameter and ionic strength of the solution also have an impact on the detergent's conformation on the nanotube surface.^[38] Nonetheless, the determination of the anhydrous specific volume by differential sedimentation can be regarded as a versatile tool to shed light on adsorption behavior.

Concerning the analysis of the average sedimentation coefficients s attributed to individualized SWCNTs, no significant deviations for HiPco-SC or HiPco-SDBS were observed. However, the sedimentation coefficients appear to be much higher for the HiPco-Per dispersions. On the one hand, this could be attributed to a lower degree of debundling in HiPco-Per. However, statistical AFM analysis of the HiPco-Per dispersions has revealed higher degrees of individualization than seen for HiPco-SDBS, as reported elsewhere.^[27,28] Furthermore, the first peak in the $c(s)$ distributions attributed to individualized nanotubes has been chosen for further analysis. On the other hand, it is quite reasonable that individualized SWCNT-Per complexes sediment more quickly than SWCNT-SC and SWCNT-SDBS, as the perylenes possess higher molecular weight. Even though the mo-

lecular weight of the surfactant has only a minor impact on the sedimentation rates of metal oxide nanoclusters,^[39] the situation is different for nanotubes, since SWCNTs are characterized by very high surface areas with low molecular weights. Thus, the molecular weight of the surfactant adsorbed even at moderate packing densities is expected to strongly influence the sedimentation coefficients. Thus, it is not surprising that the sedimentation coefficients in the case of HiPco-Per are increased to values above 20 Sv in H_2O .

Furthermore, the anhydrous molar specific volumes of the SWCNT-Per complexes deserve some attention, as they are strongly related to the packing density (the number of surfactant molecules per nm nanotube) of the surfactant on the SWCNT scaffold. Upon comparison of the two bolaamphiphilic perylene derivatives **1** and **2**, striking differences appear in the anhydrous molar volumes. Even though the bulky bolaamphiphile **2** is larger, for example, and possesses higher molecular weight, the anhydrous molar volume of SWCNT-Per2 ($0.69 \text{ cm}^3 \text{ g}^{-1}$) is significantly lower than that of SWCNT-Per1 ($0.81 \text{ cm}^3 \text{ g}^{-1}$), as summarized in Table 1. This fact is attributed to a much lower packing density of the surfactant on the SWCNT surface, which has previously been indicated by zeta-potential measurements.^[28] This observation can be understood in terms of a much higher interperylene Coulombic repulsion, as **2** is equipped with two second-generation Newkome-type dendrimers with nine carboxylic acid groups on each side of the perylene anchoring group. In contrast, compound **1** bears two first-generation Newkome dendrimers with three carboxylic acid groups on each side of the perylene core, which leads to a much reduced Coulombic repulsion. Accordingly, the perylene surfactant **1** can be more densely packed on the nanotube surface due to the reduced charge density of the polar head groups.

The result for the anhydrous molar volume of perylene **3** completes the picture. In contrast to the bolaamphiphile **2**, derivative **3** is an amphiphilic molecule, in which one second-generation Newkome dendrimer has been substituted by an alkyl chain. Thus, the surfactant can be arranged on the nanotube surface in such a way that the bulky head groups and alkyl chains alternate, as schematically depicted in Figure 8. Thus, the amphiphilic perylene derivative **3** can be more densely packed on the nanotube scaffold than **2**, which is reflected in the higher anhydrous molar volume ($0.75 \text{ cm}^3 \text{ g}^{-1}$). This adsorption pattern also accounts for the observation that the perylene surfactant **3** covers the nanotube surface more homogeneously than the bolaamphiphiles.^[28]

Nonadsorbed surfactant in micelles: As discussed above, the spatial and temporal distribution of the sedimenting species has been determined at a wavelength of 550 nm to allow the simultaneous hydrodynamic characterization of the free surfactant and the nanotubes. No significant difference in the sedimentation coefficients of the three different perylene micelles has been detected. The sedimentation coefficients in H_2O have been determined to range between 0.71 and

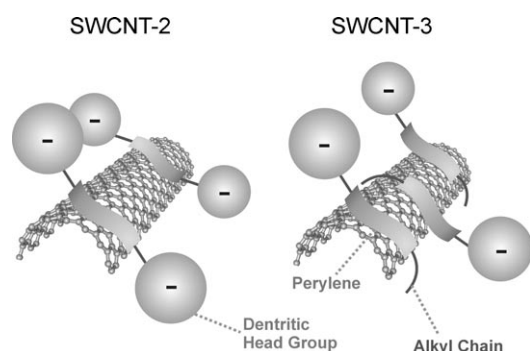


Figure 8. Schematic illustration of possible adsorption of the perylene derivatives **2** and **3**. The packing density of the amphiphile can be strongly enhanced compared with the bolaamphiphile, because an alternating arrangement of alkyl groups and dendritic head groups is accessible.

0.84 Sv. In D_2O the perylene micelles sediment even more slowly, with sedimentation coefficients between 0.10 and 0.32 Sv. The anhydrous specific volume of the perylene micelles is thus calculated to be $0.88 \text{ cm}^3 \text{ g}^{-1}$, which is in the same range as SDBS ($0.87 \text{ cm}^3 \text{ g}^{-1}$),^[40] and slightly higher than SC ($0.6 \text{ cm}^3 \text{ g}^{-1}$).^[21] Note that this is an elegant way to determine the parameters required for advanced hydrodynamic modeling of the nanotube–surfactant complexes in situ.

To determine the concentration of the free perylene molecules, we have analyzed the optical density at 550 nm after sedimentation of the nanotube species, but before discernable sedimentation of the perylene micelles. This corresponds to the last third of the Movie S1 in the Supporting Information. From the extinction coefficients, the concentration of free perylene is calculated according to Lambert–Beer's law, as summarized in Table 2. Assuming that the amount of per-

Table 2. Tabulated data for the optical density of the free perylene, the extinction coefficients $\epsilon_{550\text{nm}}$, and the resulting concentration of free perylene c_f . With knowledge of the starting concentration of the perylene c_0 (Per) and the nanotube concentration c (SWCNT), the number of moles of adsorbed perylene $n_{\text{ad}}(\text{Per})$ per g nanotubes can be calculated.

	$A_{550\text{nm}}$	$\epsilon_{550\text{nm}}$ [$\text{M}^{-1} \text{cm}^{-1}$]	d [cm]	c_f (Per) [M]	c_0 (Per) [M]	c (SWCNT) [g L^{-1}]	$n_{\text{ad}}(\text{Per})$ per g SWCNT [mmol]
2	0.43	13801	1.2	2.41×10^{-5}	4.07×10^{-5}	0.025	0.66
3	0.26	9912	1.2	2.19×10^{-5}	6.29×10^{-5}	0.023	1.70

ylene removed in the precentrifugation step is negligible, as the surface area of large bundles is much lower than for individual nanotubes and smaller bundles, the number of moles of perylene adsorbed per gram of nanotube can be deduced (see Table 2) with knowledge of the nanotube concentration and the initial perylene concentration. It can be seen that many more molecules of the amphiphilic derivative **3** are adsorbed per gram of nanotube (1.7 mmol) than the bolaamphiphile **2** (0.66 mmol per g). This finding further

supports the conclusions from the calculation of the anhydrous specific volume discussed above.

Conclusion

We have demonstrated that analytical ultracentrifugation, especially with multiwavelength detection for selective detection of various fractions, is a powerful tool for providing insights into the packing density and, therefore, the adsorption of various surfactants on the nanotube surface. From the experimentally determined sedimentation rates in water and deuterated water, the anhydrous specific volume of the SWCNT–surfactant complexes has been determined. The difference in the diameter distributions of the pristine SWCNT material (i.e., HiPco and CoMoCAT SWCNTs) is reflected by a broadened $c(s)$ distribution for the more polydisperse HiPco nanotubes. A comparison of SDBS and SC as surfactants has furthermore been related to the adsorption mechanisms previously proposed in the literature. It has been revealed that SDBS favors the “tails-on” configuration at the surfactant concentration investigated (10 g L^{-1}). From the series of nanotube–surfactant complexes we conclude that hydrodynamic modeling is not universally applicable, unless data from multiple rotational speeds is evaluated globally to suppress uncertainties in diffusion coefficients.

Concerning the analysis of the HiPco–Per dispersions, we found evidence that the bulky bolaamphiphilic derivative **2** is least densely organized on the nanotube scaffold, which is reflected in a rather low anhydrous molar volume ($0.69 \text{ cm}^3 \text{ g}^{-1}$). Among the perylene surfactants, the smallest derivative **1** is most densely adsorbed on the nanotube backbone with an anhydrous molar volume of $0.85 \text{ cm}^3 \text{ g}^{-1}$. These findings agree well with previous discussions based on zeta potential measurements.^[28] Furthermore, the amphiphilic derivative **3** yields a much higher anhydrous molar volume than the bolaamphiphile **2**. This can be rationalized by a simple adsorption scenario, in which the orientation of alkyl chains and hydrophilic head groups alternates, to allow a more dense arrangement. This is also supported by the determination of bound perylene molecules per gram of nanotubes, which is derived from the optical density of the free perylene micelles after sedimentation of the nanotubes in the analytical ultracentrifugation run.

Experimental Details

SWCNTs were obtained from Unidym (purified HiPco SWCNTs batch number P0343; purity > 95%) and SouthWest Nanotechnologies (CoMoCAT SWCNTs SG65 batch number 0012; purity > 80%) and used as received. Chemicals and solvents were purchased from Acros (Geel, Belgium), and buffer solutions from Fischer Scientific. The syntheses of the perylene bisimide derivatives were performed according to a procedure described elsewhere.^[41]

Experimentally, a model XLA (Beckman–Coulter) analytical ultracentrifuge was used to directly measure the redistribution of SWCNTs in a

centrifugal force field. This instrument enabled the characterization of the sedimentation and diffusion of SWCNTs in situ at an angular velocity of 40 krpm. Dispersed SWCNTs and reference aqueous solutions (water and deuterated water, respectively) were loaded into two-hole Epon cells equipped with quartz windows ($d=1.2$ cm). These cells were housed in a four-cell rotor (Ti-60, Beckman–Coulter), which was kept at a constant temperature of 25 °C. The optical density of the SWCNT solutions at 550 nm (unless otherwise noted) was measured as a function of time and position to track the redistribution of the SWCNTs. Experiments were typically continued for 1–2 h until essentially all the SWCNTs had sedimented to the bottom of the cells. Alternatively, we used an analytical ultracentrifuge with a multiwavelength detector that was recently developed by BASF SE and MPI Golm, described elsewhere.^[42] In short, a vacuum-compatible UV/Vis spectrometer (Ocean Optics) is placed inside the rotor chamber with suitable mechanotronics for radial scanning. The white-light source flashes in synchronization with the rotation, such that the full absorption spectrum is recorded for each radial position at each time scan. The design and the operating software (written in LabVIEW) are open source, as part of the Open-AUC work group.^[43]

The SWCNT samples in SC and SDBS in water and deuterated water were prepared as follows: HiPco SWCNTs (0.1 g L^{-1}) and CoMoCAT SWCNTs (0.2 g L^{-1}) were added to a few mL of the surfactant solution (10 g L^{-1}) and dispersed with the aid of a bath sonicator (150 W, 30 min). Coarse aggregates were removed by mild centrifugation at 15 krpm (Sigma 4 K15). The resulting dispersions were diluted with the corresponding surfactant solution to yield optical densities of approximately 1 cm^{-1} at 740 nm. The actual concentration of the SWCNTs in the dispersions subjected to analytical ultracentrifugation was calculated from the optical densities to be 0.02 g L^{-1} for the HiPco SWCNTs and 0.1 g L^{-1} for the CoMoCAT SWCNTs by using the extinction coefficients (HiPco $3625 \text{ L g}^{-1} \text{ m}^{-1}$ and CoMoCAT $950 \text{ L g}^{-1} \text{ m}^{-1}$). Unless otherwise noted, the SWCNT–Per dispersions were prepared analogously, with an initial perylene concentration of 0.1 g L^{-1} for the HiPco SWCNTs and 0.2 g L^{-1} for CoMoCAT SWCNTs in buffered aqueous media (pH 7). In the case of H_2O the phosphate buffer (ionic strength 0.09 M) was purchased from Fisher Scientific. For D_2O the buffer solution was prepared by solubilizing Na_2HPO_4 (ca. 0.42 %) and NaCl (ca. 0.11 %).

Acknowledgements

We thank Karel Planken, MPI Golm, for essential help with the evaluation of one dataset on the Ultrascan platform, Monika Page for technical assistance, and the Interdisciplinary Center for Molecular Materials (ICMM) and the Excellence Cluster Engineering of Advanced Materials (EAM) for financial support.

- [1] M. J. O'Connell, S. M. Bachilo, C. B. Huffman, V. C. Moore, M. S. Strano, E. H. Haroz, K. L. Rialon, P. J. Boul, W. H. Noon, C. Kittrell, J. Ma, R. H. Hauge, R. B. Weisman, R. E. Smalley, *Science* **2002**, 297, 593.
- [2] M. S. Arnold, S. I. Stupp, M. C. Hersam, *Nano Lett.* **2005**, 5, 713.
- [3] M. S. Arnold, A. A. Green, J. F. Hulvat, S. I. Stupp, M. C. Hersam, *Nat. Nanotechnol.* **2006**, 1, 60.
- [4] J. Crochet, M. Clemens, T. Hertel, *J. Am. Chem. Soc.* **2007**, 129, 8058.
- [5] J. Crochet, M. Clemens, T. Hertel, *Phys. Status Solidi B* **2007**, 244, 3964.
- [6] A. A. Green, M. C. Hersam, *Mater. Today* **2007**, 10, 59.
- [7] F. Hennrich, K. Arnold, S. Lebedkin, A. Quintilla, W. Wenzel, M. M. Kappes, *Phys. Status Solidi B* **2007**, 244, 3896.
- [8] J. A. Fagan, M. L. Becker, J. Chun, E. K. Hobbie, *Adv. Mater.* **2008**, 20, 1609.
- [9] A. A. Green, M. C. Hersam, *Nano Lett.* **2008**, 8, 1417.

- [10] F. Hennrich, S. Lebedkin, M. M. Kappes, *Phys. Status Solidi B* **2008**, 245, 1951.
- [11] N. Izard, S. Kazaoui, K. Hata, T. Okazaki, T. Saito, S. Iijima, N. Minami, *Appl. Phys. Lett.* **2008**, 92, 243112/1.
- [12] W.-J. Kim, N. Nair, C. Y. Lee, M. S. Strano, *J. Phys. Chem. C* **2008**, 112, 7326.
- [13] Y. Miyata, K. Yanagi, Y. Maniwa, H. Kataura, *J. Phys. Chem. C* **2008**, 112, 3591.
- [14] Y. Miyata, K. Yanagi, Y. Maniwa, H. Kataura, *Phys. Status Solidi B* **2008**, 245, 2233.
- [15] N. Nair, W.-J. Kim, R. D. Braatz, M. S. Strano, *Langmuir* **2008**, 24, 1790.
- [16] L. Wei, B. Wang, T. H. Goh, L.-J. Li, Y. Yang, M. B. Chan-Park, Y. Chen, *J. Phys. Chem. B* **2008**, 112, 2771.
- [17] K. Yanagi, T. Iitsuka, S. Fujii, H. Kataura, *J. Phys. Chem. C* **2008**, 112, 18889.
- [18] K. Yanagi, Y. Miyata, H. Kataura, *Appl. Phys. Express* **2008**, 1, 034003/1.
- [19] C. Backes, C. D. Schmidt, F. Hauke, A. Hirsch, *Chem. Commun.* **2009**, 2643.
- [20] A. Green, M. Duch, M. Hersam, *Nano Res.* **2009**, 2, 69.
- [21] M. S. Arnold, J. Suntivich, S. I. Stupp, M. C. Hersam, *ACS Nano* **2008**, 2, 2291.
- [22] W. Maechtle, L. Boerger, Springer, Berlin, **2006**.
- [23] H. Coelfen, *Anal. Ultracentrifugation* **2005**, 501.
- [24] W. Mächtle, *Makromol. Chem.* **1984**, 185, 1025.
- [25] H. G. Müller, F. Herrmann, *Prog. Colloid Polym. Sci.* **1995**, 99, 114.
- [26] P. H. Brown, P. Schuck, *Comput. Phys. Commun.* **2008**, 178, 105.
- [27] C. Backes, C. D. Schmidt, F. Hauke, C. Boettcher, A. Hirsch, *J. Am. Chem. Soc.* **2009**, 131, 2172.
- [28] C. Backes, C. D. Schmidt, K. Rosenlehner, J. N. Coleman, F. Hauke, A. Hirsch, *Adv. Mater.* **2010**, 22, 788.
- [29] C. Ehli, C. Oelsner, D. M. Guldi, A. Mateo-Alonso, M. Prato, C. Schmidt, C. Backes, F. Hauke, A. Hirsch, *Nat. Chem.* **2009**, 1, 243.
- [30] E. Karabudak, W. Wohlleben, H. Coelfen, *Eur. Biophys. J.* **2010**, 39, 397.
- [31] P. Schuck, *Biophys. J.* **2000**, 78, 1606.
- [32] SEDFIT, version 10.09b, P. Schuck, NIH, **2007**.
- [33] B. Demeler in *Analytical Ultracentrifugation: Techniques and Methods* (Eds.: D. J. Scott, S. E. Harding, A. J. Rowe), RSC, Cambridge, **2005**, p. 210.
- [34] E. Brookes, B. Demeler, *Colloid Polym. Sci.* **2008**, 286, 139.
- [35] B. Demeler, E. Brookes, L. Nagel-Stegert in *Methods in Enzymology: Computer Methods, Part A, Vol. 454* (Eds.: M. L. Johnson, L. Brand), Academic Press, London, **2009**, p. 87.
- [36] O. Matarredona, H. Rhoads, Z. Li, J. H. Harwell, L. Balzano, D. E. Resasco, *J. Phys. Chem. B* **2003**, 107, 13357.
- [37] S. Utsumi, M. Kanamaru, H. Honda, H. Kanoh, H. Tanaka, T. Ohkubo, H. Sakai, M. Abe, K. Kaneko, *J. Colloid Interface Sci.* **2007**, 308, 276.
- [38] N. R. Tummala, A. Striolo, *Phys. Rev. E* **2009**, 80, 021408/1.
- [39] E. E. Lees, M. J. Gunzburg, T.-L. Nguyen, G. J. Howlett, J. Rothacker, E. C. Nice, A. H. A. Clayton, P. Mulvaney, *Nano Lett.* **2008**, 8, 2883.
- [40] F. Tokiwa, K. Ohki, *Kolloid Z. Z. Polym.* **1968**, 223, 38.
- [41] C. D. Schmidt, C. Bottcher, A. Hirsch, *Eur. J. Org. Chem.* **2007**, 5497.
- [42] H. M. Strauss, E. Karabudak, S. Bhattacharyya, A. Kretzschmar, W. Wohlleben, H. Coelfen, *Colloid Polym. Sci.* **2008**, 286, 121.
- [43] H. Cölfen, T. Laue, W. Wohlleben, K. Schilling, E. Karabudak, B. Langhorst, E. Brookes, B. Dubbs, D. Zollars, M. Rocco, B. Demeler, *Eur. Biophys. J.* **2010**, 39, 347.

Received: December 17, 2009

Revised: July 24, 2010

Published online: September 28, 2010